Materials Transactions, Vol. 46, No. 6 (2005) pp. 1094 to 1099
Special Issue on Computer Modeling of Materials and Processes

Electronic and Lattice Properties of Layered Hexagonal Compounds Under Anisotropic Compression: A First-Principles Study

Kazuaki Kobayashi

Computational Materials Science Center, National Institute for Materials Science, 1-1, Tsukuba 305-0044, Japan

We have investigated the wurtzite and hexagonal compounds (w- and h-BN, AlN, ZnO) under various compression conditions using the first-principles molecular dynamics (FPMD) method. Applying anisotropic compression is an important approach for the investigation of novel material properties. We found remarkable changes in the internal parameters u of all calculated wurtzite compounds under uniaxial c-axis compression (P_z) within the symmetry constraint. The internal parameter u of the wurtzite structure increased as the pressure increased and finally became 0.5, resulting in a phase transformation into a hexagonal structure. Transition pressures for BN, AlN and ZnO under c-axis compression are 300–325, 15–20, 5–10 GPa, respectively. The value of the transition pressure of BN (wurtzite → hexagonal) was found to be significantly higher than those of the other two compounds (AlN, ZnO) in which the crystal structure of BN could be broken under the large uniaxial compression. The changes in the electronic band structure and the lattice properties (lattice constant, c/a ratio, volume of the unit cell) of BN in the wurtzite-to-hexagonal transformation were also quite large and unusual. These results imply that the wurtzite-to-hexagonal transformation of BN is unlikely to occur. In contrast, the changes in the lattice properties of AlN and ZnO were small because of their low transition pressures (5–20). These lower transition pressures are mainly due to larger ionicity of AlN and ZnO.

(Received December 20, 2004; Accepted April 4, 2005; Published June 15, 2005)

Keywords: *first-principles, anisotropic compression, electronic structure, wurtzite*

1. Introduction

Progress in the development of the methodology for electronic structure calculations has been remarkable in recent decades. First-principles approaches have been playing a very important role in materials science and new and epoch-making calculational methods and hardware have been developed. One of them is the "Car–Parrinello method",[1] which allows large scale calculations and practical quantum molecular dynamics. A large number of studies of the various systems (bulk, surface, interface, cluster, molecule, etc.) have given valuable results and contributions in condensed matter physics. The development of hardware has also been remarkable. One of these is the parallel computer and a variety of parallel computer systems are now available for computational material science. We perform first-principles electronic structure calculations using the HITACHI SR11000 supercomputer system (the numerical materials simulator) in NIMS in order to investigate and design electronic and lattice properties of materials.

A considerable number of theoretical and experimental studies have been made in high pressure physics. What seems to be lacking, however, is an approach for anisotropic compression. The anisotropic compression approach may reveal new information regarding the electronic and lattice properties of materials and new phases of compounds. Although it is relatively easy to treat anisotropic compression in electronic structure calculations, little attention has been given to this approach. The reason for this is the difficulty in performing the corresponding anisotropic high-pressure experiments at sufficiently low temperatures. In addition, it is necessary to prepare a large single crystal sample which is adequate for use under anisotropic compression. At the moment, the current experimental techniques almost allow the application of non-hydrostatic compression at low temperatures without using shock-compression. It is expected that theoretical results using the electronic structure calculations under anisotropic compression will be directly compared with results obtained by experiment.

In previous studies,[2–6] we found lattice anomalies in LiBC, HBC, h-MgB and C_6B_2 under anisotropic compression using the first-principles molecular dynamics (FPMD) method. These compounds all have layered hexagonal crystal structures. Lattice constants c of LiBC, HBC and C_6B_2 contract under a, b-axis compression (P_{xy}). In contrast, lattice constant a (b) of h-MgB contracts under c-axis compression (P_z). These anomalies show a kind of negative Poisson ratio. HBC, h-MgB and C_6B_2 are hypothetical compounds, while LiBC has been synthesized.[7] No experiments of LIBC have been conducted under anisotropic compression and the lattice anomaly has so far not been observed. Lattice contractions of c-axis when $P_{xy} = 50$ GPa are 0.0014 nm for LiBC, 0.0037 nm for HBC and 0.01 nm for C_6B_2, and that of a-axis when $P_z = 50$ GPa is 0.0017 nm for h-MgB. The contraction (0.01 nm) of C_6B_2 is about 1% of lattice constant c.[6]

Furthermore, a structural transformation from wurtzite to hexagonal ($w \rightarrow h$) was found in the previous study of w-MgB[8] (wurtzite structure, crystal symmetry $P6_3mc$) under uniaxial c-axis compression. This is a hypothetical compound. The transition pressure of $w \rightarrow h$-MgB (hexagonal structure, crystal symmetry $P6_3/mmc$) under c-axis compression is about 30 GPa. Therefore, we are searching for new materials which involve such lattice anomalies or structural transformations under anisotropic compression conditions. The transformation from wurtzite to hexagonal for II–VI and III–IV compounds has already been studied.[9–16] In the above studies, treated compression conditions are basically hydrostatic (isotropic) with the exception of c/a compression[10,14] mentioned later. The hexagonal phase is treated as an intermediate or metastable phase between a wurtzite → cubic (rock-salt) transformation.[10,11,14] As for w-AlN and w-ZnO, they transform into hexagonal phases under hydrostatic compression.[11,12,14] The transformation of

$h \rightarrow w$-BN under hydrostatic compression was observed in a high pressure experiment[17,18] and has been theoretically studied.[19,20]

At first, we investigated w-BN as one of the candidates. Although there are no lattice anomalies of w-BN under anisotropic compression, we found the structural transformation from w-BN to h-BN under c-axis compression, as shown in Fig. 1. Furthermore, we examined w-AlN and w-ZnO in this paper. These two compounds also show the transformation from wurtzite to hexagonal under c-axis compression. The transition pressure of w-BN under c-axis compression is quite large. The $w \rightarrow h$ transformation of BN under hydrostatic compression is unlikely because the total energy of h-BN in the range of high pressure is higher and unfavorable energetically than that of w-BN.[21,22] In contrast, the transition pressures of AlN and ZnO from wurtzite to hexagonal under c-axis compression are lower than those under hydrostatic compression.[11,12,14]

2. Method of Calculation

The present calculation is based on the local density approximation (LDA) in density functional theory[23,24] with von-Barth and Hedin[25] (for BN), Wigner[26] (for AlN) and Perdew and Zunger[27,28] (for ZnO) interpolation formulae for exchange-correlation. The optimized pseudopotentials by Troullier and Martins (TM)[29,30] were used. Zn treats $3d$ states as valence states. A partial core correction (PCC)[31] was considered for the Al pseudopotential. Nonlocal parts of the pseudopotentials were transformed to the Kleinman-Bylander separable forms[32] without ghost bands. The number of sampling k-points was 95 in the irreducible Brillouin zone (BZ). The wave function was expanded in plane waves, and the energy cutoff was 144 Ry for BN and 81 Ry for AlN, ZnO with the maximum number of plane waves being about 11000 for BN. The number of atoms in the unit cell is 4 for the wurtzite and hexagonal structures. The crystal structures of wurtzite ($P6_3mc$) and hexagonal ($P6_3/mmc$) are shown in Fig. 1. It is noted that $P6_3mc$ (184) is a subgroup of the $P6_3/mmc$ (194) space group.

The optimization of the electronic and lattice properties was performed by a modified version of the FPMD that originated from the Car–Parrinello method.[1] An iterative update of the electronic wave function was carried out using a modified version of the steepest descent type of algorithm proposed by Williams and Soler.[33] An internal parameter u of the wurtzite crystal structure in the unit cell was optimized by Hellmann-Feynman forces acting on atoms. Our criterion for optimizing the internal coordinates of atoms was that the maximum force acting on each atom should be less than 5.0×10^{-4} Ry/Bohr.

The lattice parameters were optimized by stresses.[34] We set external stresses acting on unit cell surfaces in order to optimize the lattice constants. Internal stresses were obtained by the following formulae,

$$\sigma_{\alpha\beta} = \frac{1}{\Omega} \frac{\partial E_{\mathrm{tot}}}{\partial \varepsilon_{\alpha\beta}} \tag{1}$$

where $\sigma_{\alpha\beta}$ is a stress tensor, α, β denote Cartesian coordinates (x, y, z), Ω is the volume of the unit cell, E_{tot} is

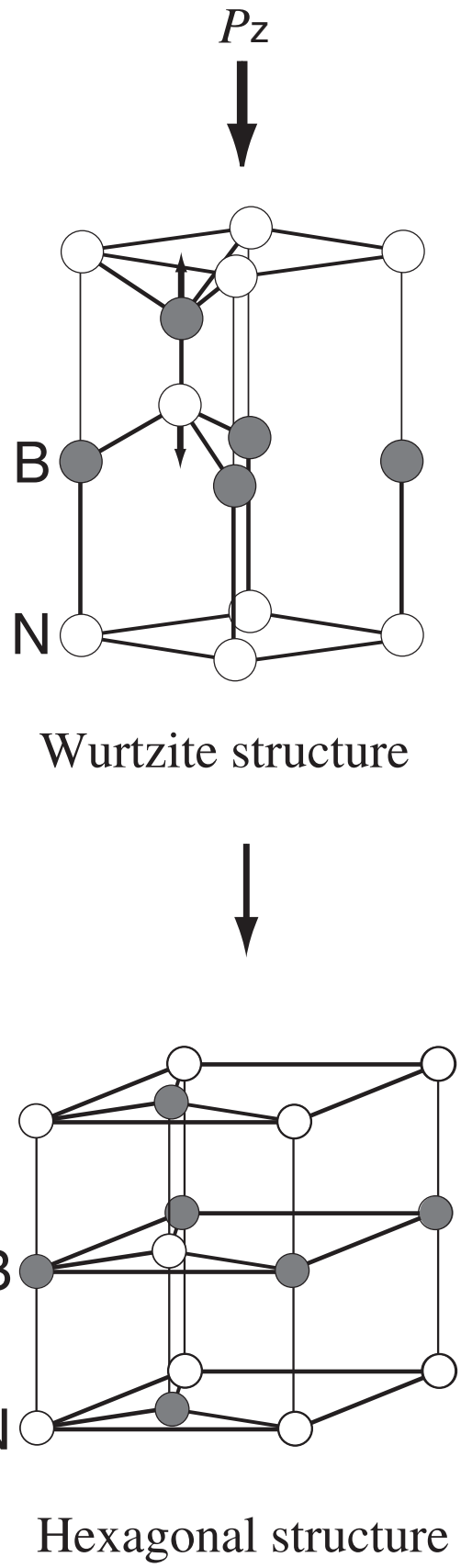

Fig. 1 Crystal structures of wurtzite and hexagonal. An arrow with P_z indicates the uniaxial c-axial compression. Internal B (Al, Zn) and N (O) atoms in the unit cell vary along the arrowed directions under c-axis compression, indicating the transformation from wurtzite to hexagonal under c-axis compression.

the total energy and ε is the strain. The lattice properties are tuned by coincidence of internal and external compressions in the process of FPMD as follows,

$$P_{\text{int}} = P_{\text{ext}}, \tag{2}$$

where P_{int} (P_{ext}) is internal (external) compression. We examined the hydrostatic, uniaxial (c-axis) and biaxial (a, b-axis) compression conditions. Hydrostatic compression is defined as

$$P = -\sigma_{xx} = -\sigma_{yy} = -\sigma_{zz}. \tag{3}$$

Uniaxial compression along c-axis is defined as

$$P_z = -\sigma_{zz}, \tag{4}$$

when external compressions of $P_{\text{ext}}x = P_{\text{ext}}y = 0$ GPa.

Biaxial compression in the a, b-plane (a, b-axis) is defined as

$$P_{\text{xy}} = -\sigma_{xx} = -\sigma_{yy}, \tag{5}$$

when external compression of $P_{\text{ext}}z = 0$ GPa. Our criterion for optimizing the unit cell surfaces is that the maximum pressure acting on each unit cell surface should be less than 0.03 GPa, which corresponds to an alteration of less than 0.0001 nm in the optimization of the lattice constant. Off-diagonal terms of the stress tensor were not considered. The number of k-points was fixed during the cell optimization.

Structural phase transition, crystallinity break, interlayer gliding, etc. were not considered in the process of the FPMD, with the exception of the wurtzite $\rightarrow$ hexagonal transformation. The crystal symmetry of each phase was kept under compression in this study. The purpose of our study was to obtain the final stable structure under each compression condition. Although the pseudopotentials used in the FPMD calculation do not take into account the effect of core electrons, the influence of core states is small in this study.

3. Results and Discussion

The optimized lattice properties of wurtzite (w-) and hexagonal (h-) phases for BN, AlN and ZnO under various compression conditions are tabulated in Table 1. h-BN, AlN and ZnO were calculated in order to compare them with the results of w-BN, AlN and ZnO. The equilibrium lattice constants agree with the experimental results.[35–37] Hydrostatic (P), uniaxial (P_z) and biaxial (P_{xy}) compressions were applied to w-BN. Hydrostatic and uniaxial compressions were applied to w-AlN, w-ZnO and h-BN. Hydrostatic compression was applied to h-AlN, h-ZnO.

We found that the wurtzite structure of BN transformed into a hexagonal structure when $P_z = 325$ GPa, as shown in Fig. 1. Such a transformation was also found in previous studies[8] of w-MgB. A transformation from wurtzite to hexagonal under c/a compression was reported.[10,14] The lattice parameters were relaxed for each c/a ratio with considerable uniaxial strain in the c direction in c/a compression. This compression is different than the application of uniaxial external compression with the cell optimization (c/a variable) in this study. The $w \rightarrow h$ transformation occurred under uniaxial c-axis compression in the present work. The crystal symmetry of w-BN was artificially maintained in the process of the $w \rightarrow h$ transformation. The internal parameter u varied from 0.3744 ($P = 0$ GPa) to 0.5 ($P_z = 325$ GPa) under c-axis compression. The value of u when $P_z = 300$ GPa was 0.4125 and the wurtzite structure was retained, as shown in Table 1. The value (0.5) of u when $P_z = 325$ GPa means the crystal structure is hexagonal. In the same way, w-AlN transformed into h-AlN ($u \rightarrow 0.5$) when $P_z = 20$ GPa. This transition pressure ($P_z = 15$–20 GPa) of AlN under c-axis compression is smaller than that ($P_z =$ 300–325 GPa) of BN. This trend is the same as that found for w-ZnO. We confirmed that these transformations of BN, AlN, ZnO occur when $P_z = 325$, 20 and 10 GPa, respectively. Therefore, the transition pressures of BN, AlN, ZnO under c-axis compression are roughly estimated to be 300–325, 15–20 and 5–10 GPa, respectively. As for w-AlN and w-ZnO under hydrostatic compression (P), we found that they transformed into hexagonal phases when $P = 50$–100 GPa for AlN and $\sim$50 GPa for ZnO. This trend is consistent with previous results ($P \approx 75$ GPa for AlN.[11] and 20 GPa for ZnO[12]). However, the transition pressure of AlN under

Table 1 Optimized lattice constants[nm], the c/a ratios of w and h-BN, AlN, ZnO and internal parameters u of the wurtzite structure. "BH", "W" and "PZ" indicate the LDA formulae by von Barth and Hedin,[25] Wigner[26] and Perdew and Zunger,[27,28] respectively. "$w \rightarrow h$" indicates the structural transformation from wurtzite to hexagonal. "Exp" denotes experimental values.

	GPa	c	a	c/a	u
w-BN(BH)	$P = 0$	0.4164	0.2516	1.655	0.3744
w-BN(BH)	$P = 50$	0.4024	0.2429	1.657	0.3737
w-BN(BH)	$P_{xy} = 50$	0.4182	0.2421	1.727	0.3725
w-BN(BH)	$P_z = 50$	0.3995	0.2522	1.584	0.3763
w-BN(BH)	$P_z = 200$	0.3610	0.2551	1.415	0.3908
w-BN(BH)	$P_z = 300$	0.3343	0.2606	1.282	0.4125
$w \rightarrow h$-BN(BH)	$P_z = 325$	0.2144	0.5593	0.383	0.5
w-BN(Exp[35])	$P = 0$	0.4220	0.2553	1.653	
h-BN(BH)	$P = 0$	0.6568	0.2478	2.651	
h-BN(BH)	$P = 50$	0.4690	0.2419	1.939	
h-BN(BH)	$P = 200$	0.3749	0.2337	1.604	
h-BN(BH)	$P_z = 50$	0.4514	0.2503	1.804	
h-BN(BH)	$P_z = 325$	0.2144	0.5593	0.383	
h-BN(Exp[35])	$P = 0$	0.6656	0.2504	2.658	
w-AlN(W)	$P = 0$	0.5034	0.3136	1.605	0.3811
w-AlN(W)	$P = 50$	0.4674	0.2971	1.573	0.3874
$w \rightarrow h$-AlN(W)	$P = 100$	0.3770	0.3050	1.236	0.5
w-AlN(W)	$P_z = 15$	0.4719	0.3187	1.481	0.4012
$w \rightarrow h$-AlN(W)	$P_z = 20$	0.3942	0.3385	1.165	0.5
w-AlN(Exp[36])	$P = 0$	0.4980	0.3110	1.601	0.3821
h-AlN(W)	$P = 0$	0.4205	0.3324	1.265	
h-AlN(W)	$P = 50$	0.3920	0.3157	1.242	
w-ZnO(PZ)	$P = 0$	0.5259	0.3268	1.609	0.3798
$w \rightarrow h$-ZnO(PZ)	$P = 50$	0.4125	0.3276	1.259	0.5
w-ZnO(PZ)	$P_z = 5$	0.4973	0.3334	1.491	0.4033
$w \rightarrow h$-ZnO(PZ)	$P_z = 10$	0.4202	0.3543	1.186	0.5
w-ZnO(Exp[37])	$P = 0$	0.52066	0.32498	1.6021	0.3832
h-ZnO(PZ)	$P = 0$	0.4446	0.3473	1.280	
h-ZnO(PZ)	$P = 50$	0.4125	0.3276	1.259	

hydrostatic compression does not agree with the result ($P = 24.7$ GPa).[14]

Since the interlayer distance contracts and the intralayer distance expands under c-axis compression (P_z), the internal parameter u increased as P_z increased and finally became 0.5 as shown in Fig. 1. This transformation ($u \to 0.5$) is related to a change in coordination number ($4 \to 5$) and ionicity of BN, AlN and ZnO as mentioned later in detail. The transition pressure of BN under c-axis compression is significantly larger than that of AlN and ZnO. The changes in the lattice properties (lattice constant, c/a ratio) of BN at the $w \to h$ transformation ($P_z = 325$ GPa) under c-axis compression were also significant (= Table 1). In contrast, the changes in the lattice properties of AlN and ZnO were only small. The volume of h-BN when $P_z = 325$ GPa is 2.95 times greater than that of w-BN when $P_z = 300$ GPa. The density of h-BN at the structural transformation point was lower than that of w-BN when $P_z = 300$ GPa. The lattice parameters (lattice constants a, c, c/a ratio) of BN at the $w \to h$ transformation ($P_z = 325$ GPa) under c-axis compression coincided with the values of h-BN which is optimized when $P_z = 325$ GPa as the initial structure was hexagonal (Table 1). The interlayer distance of h-BN when $P_z = 325$ GPa was found to be 0.1072 nm. This value corresponds to the shortest bond length and is extremely small. The intralayer distance of a B–N bond when $P_z = 325$ GPa was determined to be 0.3229 nm. This value is 2.2 times as great as that when $P = 0$ GPa. This unusual volume increase and significant changes in lattice properties at the $w \to h$ transformation implies that it would be unlikely to occur under c-axis compression for BN. It is likely that the crystal structure of w-BN is broken under such a large compression condition.

In contrast, the volume of h-AlN under $P_z = 20$ GPa was found to be 0.94 times as large as that of w-AlN when $P_z = 15$ GPa, which means the density of AlN increases at the $w \to h$ transformation under c-axis compression. Similarly, the volume of h-ZnO when $P_z = 10$ GPa was 0.95 times as large as that of w-ZnO when $P_z = 5$ GPa.

This remarkable difference in the changes in lattice properties between BN and the other two compounds (AlN, ZnO) is related to their relative ionicities. The ionicity of AlN and ZnO is higher than that of BN. A larger coordination number is favorable in the ionic bonds of the crystal. The coordination numbers of wurtzite and hexagonal phases are 4 and 5, respectively. Although the coordination number of the rock-salt (rs) phase is 6, it was not considered in this study. Particularly, all coordinated bond lengths of the hexagonal phase are equal when c/a is $2/\sqrt{3} = 1.155$ (≈ 1.2[10]). As for AlN and ZnO, the $w \to h$ transformation occurred when c/a is around 1.2 and increasing the coordination number is energetically favorable due to their ionicity. In fact, the c/a ratios of h-AlN and h-ZnO when $P = 0$ GPa were 1.265 and 1.280, respectively. Although the c/a ratio of w-AlN and w-ZnO when $P = 0$ GPa were 1.605 and 1.609, respectively, they became below 1.2 at the lower transition pressure ($P_z = 10$–20 GPa) under c-axis compression as shown in Table 1. An interlayer interaction of h-BN is weak due to lack of ionicity although the intralayer interaction is strong. Therefore, the c/a ratio of h-BN when $P = 0$ GPa was 2.651, two times larger than those of h-AlN and h-ZnO. The c/a ratio of h-BN under c-axis compression decreased extremely due to this weak interlayer interaction. Although the c/a ratio of w-BN converged to the value of 1.2 when $P_z = 300$, it changed rapidly to 0.383 at the $w \to h$ transformation ($P_z = 325$ GPa) under c-axis compression.

We calculated the electronic band structures of w-BN, AlN and ZnO. They are non-metallic. The values of the band gap of w-BN, AlN and ZnO when $P = 0$ GPa were found to be about 4–5, 4, and 0.6 eV, respectively. These values are smaller than those determined by experiment. Values of the band gap are usually underestimated in the DFT-LDA calculation. The bandwidth increased as the pressure increased in all cases, with the exception of h-BN when $P_z = 325$ GPa. The electronic band structures of w-BN when $P = 0$ GPa, $P_z = 300$ GPa and 325 GPa ($w \to h$) are shown in Fig. 2, respectively. Although the Brillouin zone of BN varied remarkably under the structural transformation, the horizontal scales were adjusted to give the same length for each symmetric line with different lattice constants so that they can be schematically compared. Since the crystal structure of w-BN when $P_z = 300$ GPa was retained, the change in the electronic band structures was small. The change in the electronic band structure when $P_z = 325$ GPa was remarkable in comparison with those when $P = 0$ GPa and $P_z = 300$ GPa. This electronic band structure is obviously insubstantial, which implies that the $w \to h$ transformation is unlikely, as already mentioned.

In contrast, the electronic band structures of w-AlN when $P = 0$ GPa, $P_z = 15$ GPa and 20 GPa ($w \to h$) are mostly invariant as shown in Fig. 3. Overall, the electronic band structures of w-BN and w-AlN resemble each other. The electronic band structures of w-ZnO when $P = 0$ GPa, $P_z = 5$ GPa and 10 GPa ($w \to h$) are shown in Fig. 4. They are also mostly invariant in each compression condition. 3d states of Zn are located at 5–6 eV below the top of the valence bands. The electronic band structures of w-ZnO and the other two compounds (w-BN, w-AlN) resemble each other with the exception of the Zn 3d states. The band gap of h-AlN when $P_z = 20$ GPa is narrower than that of w-AlN when $P = 0$ GPa. In contrast, the band gap of h-ZnO when $P_z = 10$ GPa is slightly wider than that of w-ZnO when $P = 0$ GPa.

4. Summary

We calculated the electronic and lattice properties of w- and h-BN, AlN, ZnO under various compression conditions using FPMD. In this study, we were unable to find the anomalous behavior[2–6] of their lattice constants. We found that the structural phase transformation from wurtzite to hexagonal occurred under c-axis compression. The internal parameter u changed finally to 0.5 under c-axis compression. The transition pressures of $w \to h$-BN, AlN and ZnO under c-axis compression was found to be 300–325 GPa, 15–20 GPa and 5–10 GPa, respectively. There is the large difference of the transition pressure between BN and other two compounds. Particularly, the volume (density) of BN increased (decreased) at the $w \to h$ transformation. Therefore, the bandwidth of BN decreases because of increasing volume. In contrast, the densities of AlN and ZnO increased

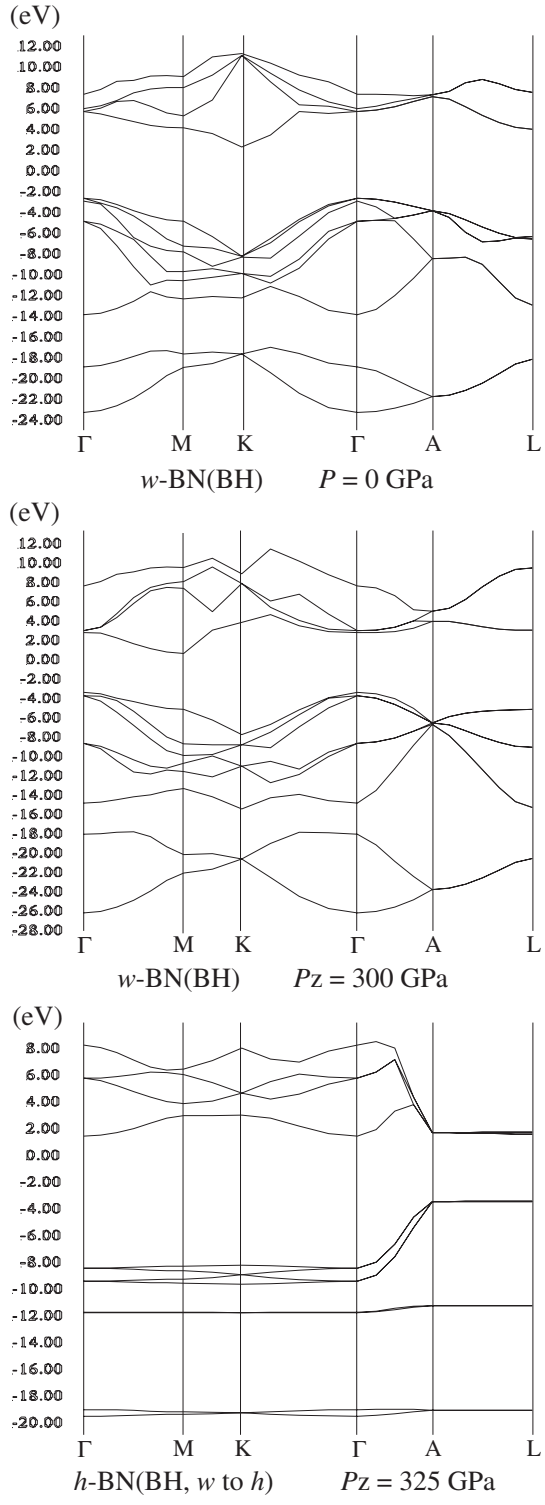

Fig. 2 Energy band structures of w-BN when $P = 0$, and $P_z = 300$, 325 GPa. w-BN transforms into h-BN when $P_z = 325$ GPa.

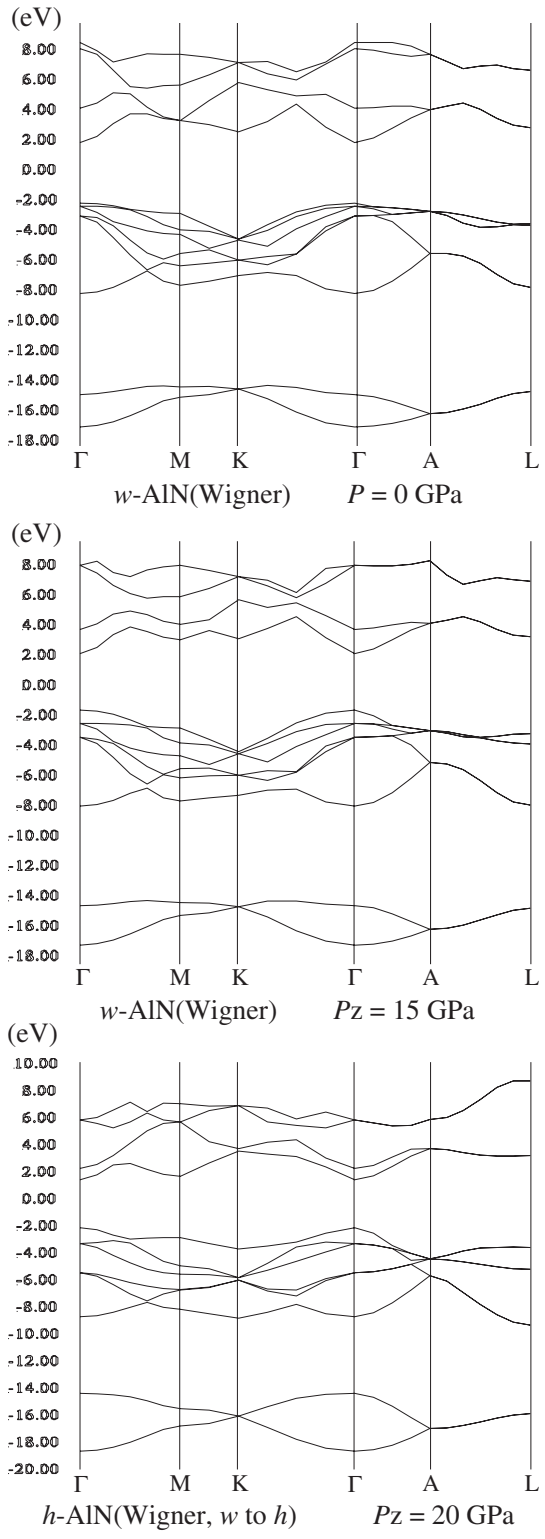

Fig. 3 Energy band structures of h-AlN when $P = 0$ and $P_z = 15$, 20 GPa. w-AlN transforms into h-AlN when $P_z = 20$ GPa.

at the $w \rightarrow h$ transformation. The change in the electronic band structure of BN after the transformation is noteworthy when compared with those of w-AlN and w-ZnO. The quite large transition pressure and remarkable changes in the electronic and lattice properties of BN implies that the $w \rightarrow h$ transformation under compression is unlikely. In BN, lower ionicity and the large value (2.651) of c/a of the hexagonal phase may play an important role in the unusually high transition pressure. Since the transition pressures of w-AlN and ZnO under c-axis compression are smaller than those under hydrostatic compression,[11,12,14] it may be possible to observe experimentally the $w \rightarrow h$ transformations under c-axis compression. It is expected that the $w \rightarrow h \rightarrow$ *cubic* (*rs*) transformation of AlN, ZnO and related compounds under anisotropic compression will be realized. More detailed

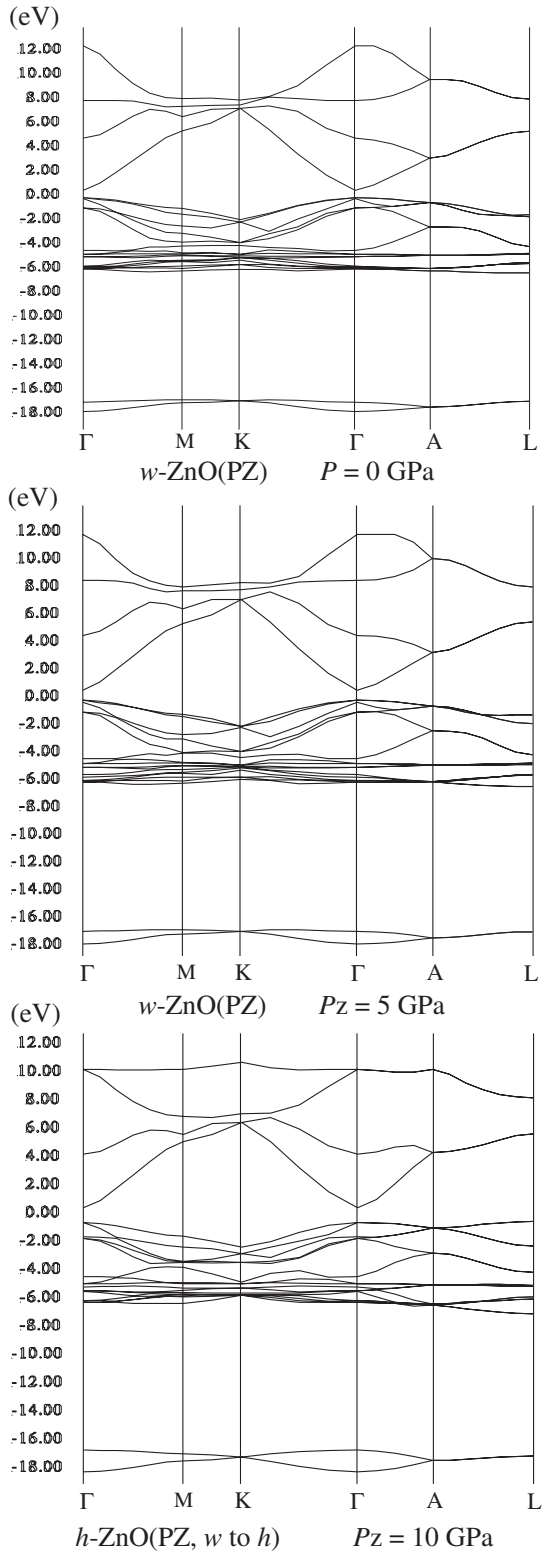

Fig. 4 Energy band structures of *h*-ZnO when $P = 0$ and $P_z = 5$, 10 GPa. *w*-ZnO transforms into *h*-ZnO when $P_z = 10$ GPa.

calculations of present and related compounds with the wurtzite and hexagonal structures are necessary for future work. It is necessary to consider the transformation from wurtzite (hexagonal) to cubic phases. We believe that the study of anisotropic compression will be increasingly important in materials science and design in the near future.

Acknowledgements

The valuable discussions and advice of Dr. T. Taniguchi and Dr. K. Watanabe in this study are gratefully acknowledged. The numerical calculations were performed at The National Institute for Materials Science (AlphaServer GS140 [HP] and the numerical materials simulator [SR11000, HITACHI]).

REFERENCES

1) R. Car and M. Parrinello: Phys. Rev. Lett. **55** (1985) 2471–2474.
2) K. Kobayashi and M. Arai: Physica C **388–389** (2003) 201–202.
3) K. Kobayashi and M. Arai: J. Phys. Soc. Jpn. **72** (2003) 217–220.
4) K. Kobayashi, M. Arai and T. Sasaki: Trans. MRS-J. **29** (2004) 3799–3802.
5) K. Kobayashi and M. Arai: Mater. Trans. **45** (2004) 1465–1468.
6) K. Kobayashi, Y. Zenitani and J. Akimitsu: to be submitted in proceedings of ISS2004 (Physica C).
7) M. Wörle, R. Nesper, G. Mair, M. Schwarz and H. G. von Schnering: Z. Anorg. Allg. Chem. **621** (1995) 1153–1159.
8) K. Kobayashi, M. Arai and K. Yamamoto: J. Phys. Soc. Jpn. **72** (2003) 2886–2892.
9) W. R. L. Lambrecht, S. Limpijumnong and B. Segall: MRS Internet J. Nitride Semicond. Res. **4S1** (1999) G6.8.
10) S. Limpijumnong and W. R. L. Lambrecht: Phys. Rev. Lett. **86** (2001) 91–94.
11) J. Serrano, A. Rubio, E. Hernandez, A. Munoz and A. Mujica: Phys. Rev. B **62** (2000) 16612.
12) F. Decremps, F. Datchi, A. M. Saitta, J. P. Itie, A. Polian, F. Baudelet and S. Pascarelli: *High Pressure Research* **22** (2002) 365–367.
13) J. Serrano, A. H. Romero, F. J. Manjon, R. Lauck, M. Cardona and A. Rubio: Phys. Rev. B **69** (2004) 094306.
14) A. M. Saitta and F. Decremps: Phys. Rev. B **70** (2004) 035214.
15) S. Linpijumnong and S. Jungthawan: Phys. Rev. B **70** (2004) 054104.
16) P. E. Van Camp, V. E. Van Doren and J. T. Devreese: Phys. Rev. B **44** (1991) 9056–9059.
17) J. R. Riter, Jr.: J. Chem. Phys. **59** (1973) 1538–1538.
18) Y. Meng *et al.*: Nature Materials **3** (2004) 111–114.
19) R. M. Wentzcovitch, S. Fahy, M. L. Cohen and S. G. Louie: Phys. Rev. B **38** (1988) 6191–6195.
20) W. J. Yu, W. M. Lau, S. P. Chan, Z. F. Liu and Q. Q. Zheng: Phys. Rev. B **67** (2003) 014108.
21) Y. Xu and W. Y. Ching: Phys. Rev. B **44** (1991) 7787–7798.
22) J. Furthmuller, J. Hafner and G. Kresse: Phys. Rev. B **50** (1994) 15606–15622.
23) P. Hohenberg and W. Kohn: Phys. Rev. **136** (1964) B864–B871.
24) W. Kohn and L. J. Sham: Phys. Rev. **140** (1965) A1133–A1138.
25) U. von Barth and L. Hedin: J. Phys. C **5** (1972) 1629–1642.
26) E. Wigner: Phys. Rev. **46** (1934) 1002–1011.
27) J. Perdew and A. Zunger: Phys. Rev. B **23** (1981) 5048–5079.
28) D. M. Ceperley and B. J. Alder: Phys. Rev. Lett. **45** (1980) 566–569.
29) N. Troullier and J. L. Martins: Phys. Rev. B **43** (1991) 1993–2006.
30) K. Kobayashi: Mater. Trans. **42** (2001) 2153–2156.
31) S. G. Louie, S. Froyen and M. L. Cohen: Phys. Rev. B **26** (1982) 1738–1742.
32) L. Kleinman and D. M. Bylander: Phys. Rev. Lett. **48** (1982) 1425–1428.
33) A. R. Williams and J. Soler: Bull. Am. Phys. Soc. **32** (1987) 562.
34) O. H. Nielsen and R. M. Martin: Phys. Rev. B **32** (1985) 3792–3805.
35) O. Mishima and K. Era: Electric Refractory Materials, ed. by Y. Kumashiro, (2000) 495–556.
36) H. Schulz and K. Thiemann: Solid State Commun. **23** (1977) 815–819.
37) S. Desgreniers: Phys. Rev. B **58** (1998) 14102–14105.